Fe-N-Modified Multi-Walled Carbon Nanotubes for Oxygen Reduction Reaction in Acid

Hye Ryung Byon[a,b,c], *Jin Suntivich*[b,c], *Ethan J. Crumlin*[a,c], *and Yang Shao-Horn*[a,b,c]*

[a]Department of Mechanical Engineering

[b]Department of Materials Science and Engineering

[c]Electrochemical Energy Laboratory

Massachusetts Institute of Technology,

Cambridge, MA 02139, USA

E-mail: shaohorn@mit.edu

Extended X-ray Absorption fine structure (EXAFS) analysis. The refined values of the $\chi_{Fe\text{-}Fe}$ and $\chi_{Fe\text{-}N}$, which encompass the passive electron reduction values ($S^2_{Fe\text{-}Fe}$ and $S^2_{Fe\text{-}N}$) and the mean square displacement ($\sigma^2_{Fe\text{-}Fe}$ and $\sigma^2_{Fe\text{-}N}$) determined from the reference compound fitting, were used as constants in the Fe-N-MWCNT EXAFS fitting. To fit the Fe-N-MWCNT EXAFS, the model Fe-N$_4$ planar structure with variable $cCN_{Fe\text{-}N}$ (corrected Fe-N coordination number ratio, defined as the ratio between the experimental Fe-N coordination ($CN_{Fe\text{-}N,exp}$) and the ideal Fe-N coordination number ($CN_{Fe\text{-}N,theory}$), which is 4 for the square-planar model, *vide infra*) was used, where the Fe-N distance was initially set to 1.972Å, in addition to the first two Fe-Fe paths of the Fe body-centered cubic (bcc) structure. Note that Fe-Cl and Fe-O paths were neglected in our calculation owing to its negligible concentration after the heat treatment and acid-leaching. Therefore, assuming that the scattering path shell consists predominantly of two sub-paths (Fe-N and Fe-Fe), the total scattering path of the first shell, χ, was calculated by the following:

$$\chi_{total} = (x)cCN_{Fe-N}(\chi_{Fe-N}) + (1-x)cCN_{Fe-Fe}(\chi_{Fe-Fe}) \qquad \text{(eq. S1)}$$

$$= A\chi_{Fe-N} + B\chi_{Fe-Fe}$$

$$A = (x)cCN_{Fe-N}$$

$$B = (1-x)cCN_{Fe-Fe}$$

where cCN is the corrected coordination number ratio ($cCN = CN_{exp}/CN_{theory}$) and x is the fraction of Fe-N in the system. Using equation S1 and the fitted values of A and B, $CN_{Fe\text{-}N,exp}$ of Fe-N-MWCNT was calculated from the following.

$$CN_{Fe-N,\exp} = cCN_{Fe-N} \cdot CN_{Fe-N,theory}$$

$$= \frac{cCN_{Fe-Fe}(x)A}{(cCN_{Fe-Fe} - B)} CN_{Fe-N,theory} \qquad \text{(eq. S2)}$$

When $cCN_{Fe\text{-}Fe}$ is set to 1 (Fe bulk phase assumption), $CN_{Fe\text{-}N,theory}$ is referred from the FeTMPP-Cl fitting, and A and B values are obtained from the Fe-N-MWCNT measured, the $CN_{Fe\text{-}N,exp.}$can be estimated.

Fig. S1 Molecular structure scheme of heterocyclic N compounds.[1]

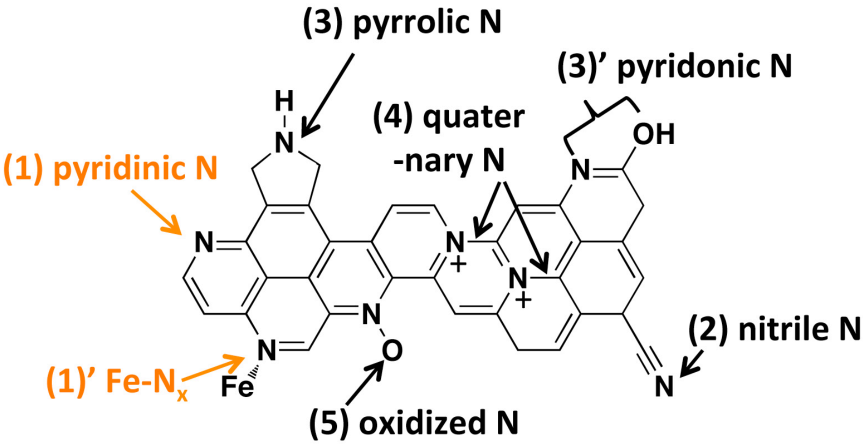

Fig. S2 XPS of 3-Fe-N-MWCNT in (a) survey and (b) Fe 2p BE regions. The dashed box in (a) is the Fe 2p BE region.

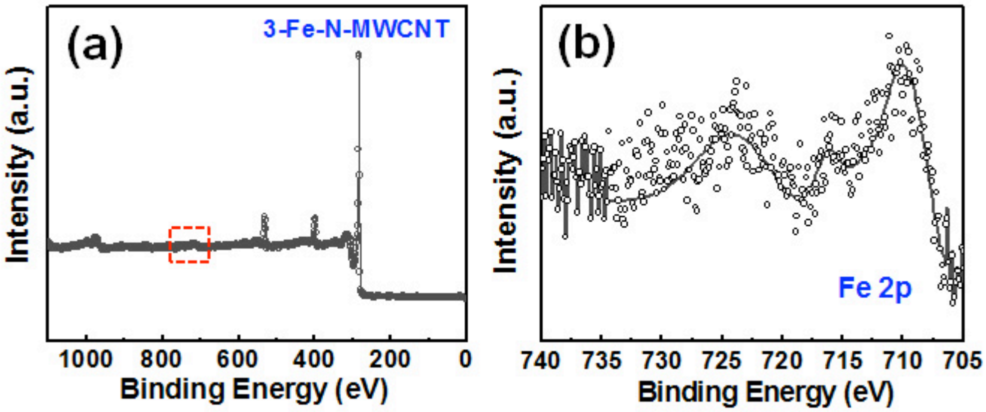

Fig. S3 XRD patterns (Cu Kα = 1.5218 Å, Rigaku) of background (black), N-MWCNT (orange), 2-Fe-N-MWCNT (green), and 3-Fe-N-MWCNT (blue). The peak at 25.8^{o} (0.34 nm) corresponds to the (002) stacking of the graphitic carbon. The triangle symbols in the gray box area indicate the background peaks from the XRD sample holder and the adhesive.

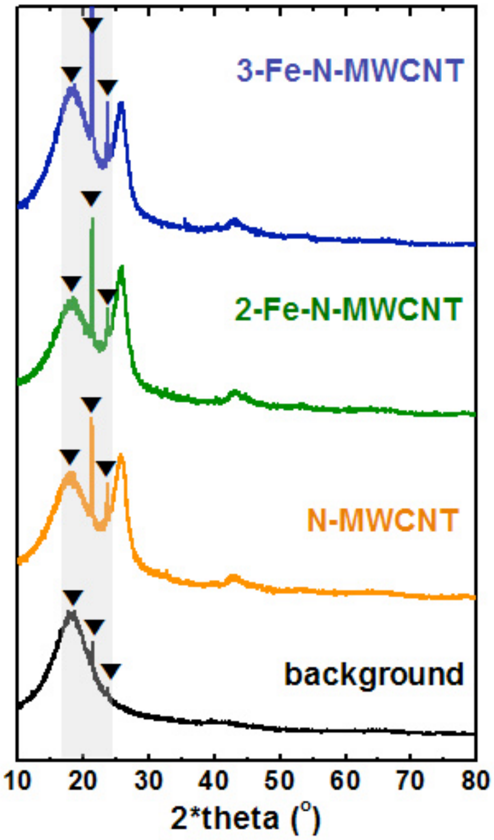

Fig. S4 High-resolution TEM (HRTEM) images of 3-Fe-N-MWCNT after acid-leaching in 2 M H_2SO_4 at 80 ^oC for 3 hours. (b-d) The 3-Fe-N-MWCNT has a Fe nanoparticle impurity encased inside MWCNT. Image of (d) is a high magnification of (c).

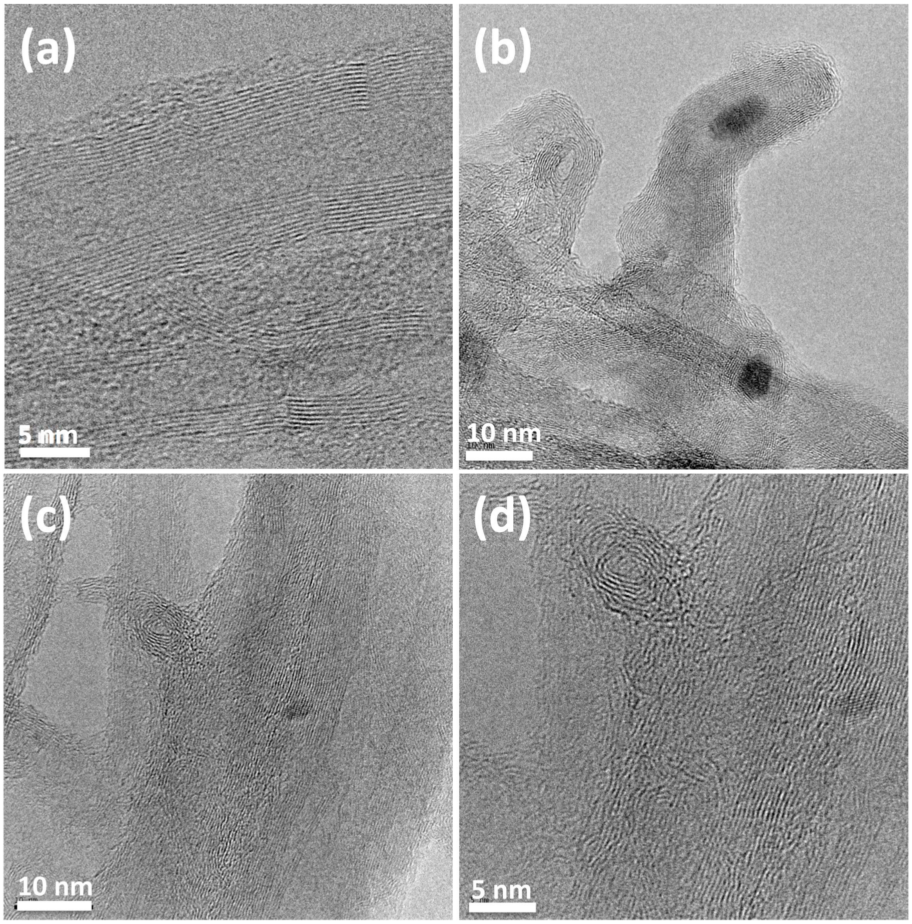

Fig. S5 SEM images of (a – b) 2-Fe-N-MWCNT, and (c – d) 3-Fe-N-MWCNT powders. Images of (b) and (d) are high magnifications of (a) and (c), respectively.

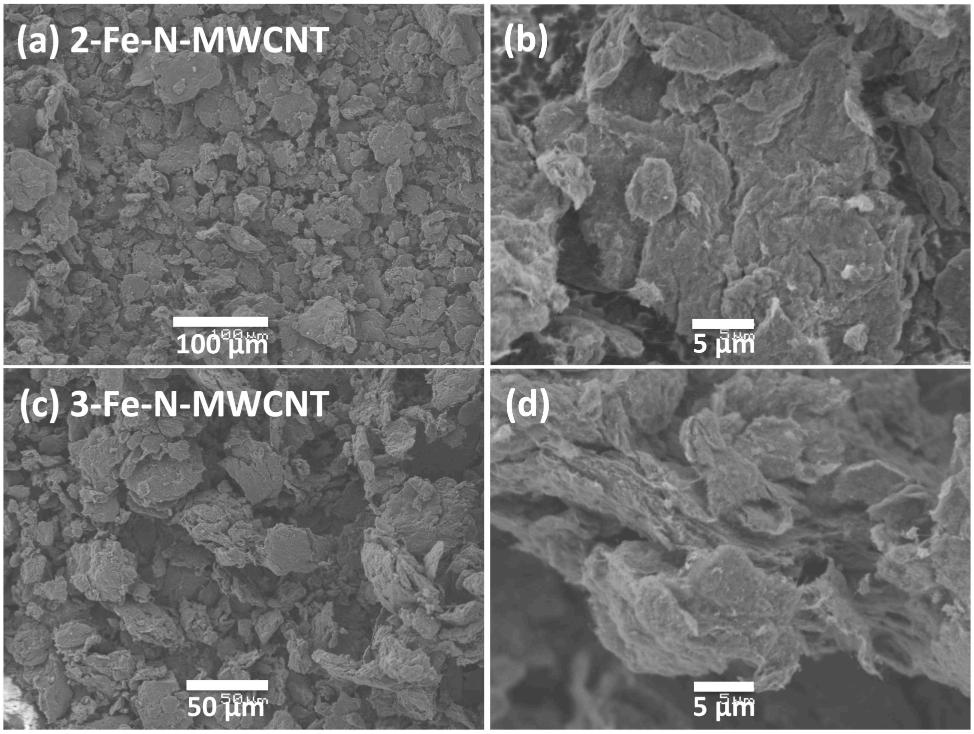

Fig. S6 Polarization curves of (a) Pt-RDE, (b) N-MWCNT, (c) 1-Fe-N-MWCNT, (d) 2-Fe-N-MWCNT, and (e) 3-Fe-N-MWCNT in O_2-saturated 0.5 M H_2SO_4 at 10 mV s^{-1} (loading: 0.4 $mg_{catalyst}\ cm^{-2}_{geo}$). The rotation rates are 100 (green), 400 (blue), 900 (pink), 1600 (red), and 2500 (black) rpms.

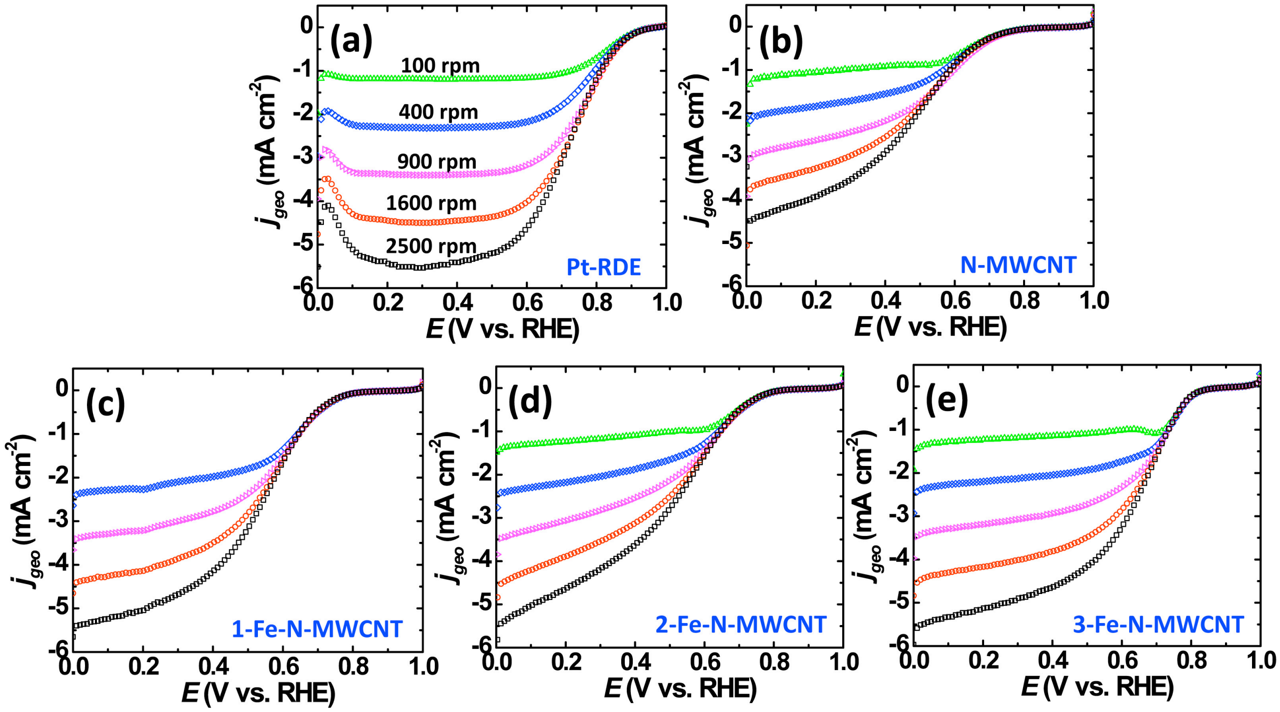

Fig. S7 Polarization curves of pristine MWCNT-NH_2 (blue open diamond), HT-MWCNT-NH_2 (pink open square), and N-MWCNT (orange solid circle) in O_2-saturated 0.5 M H_2SO_4 at 10 mV s^{-1} and 900 rpm (loading: 0.4 $mg_{catalyst}$ cm^{-2}_{geo}). The HT-MWCNT-NH_2 was prepared by annealing of the pristine MWCNT-NH_2 at 800 °C for 2 hours in Ar gas flowing.

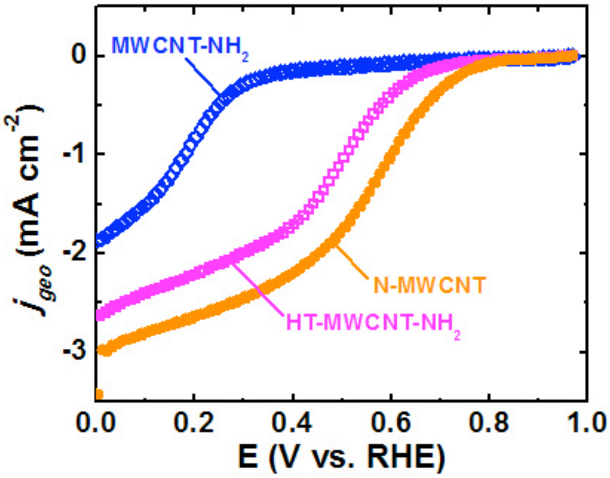

Fig. S8 XPS of (a) pristine MWCNT-NH_2, and (b) HT-MWCNT-NH_2 in the N 1s BE region. The intensities of (a) and (b) are normalized by the ones of carbon sp^2 peaks (294.5 eV) and (b) is magnified to 5 times. The numbers in (b) indicate heterocyclic N molecules such as 1 : pyridinic N (~398.5 eV), 1' : Fe-N_4 obtained from FeTMPP-Cl (~398.5 eV), 2 : nitrile N (~399.8 eV), 3 : pyrrolic N (~400.3 eV), 3' : pyridonic N (~400.3 eV), 4 : quaternary N (~401.4 eV), and 5 : oxidized N (402 ~ 405 eV)[2,3] while (a) shows amine and amide groups[4, 5]. The atomic N/C ratio are (a) 0.056 and (b) 0.004.

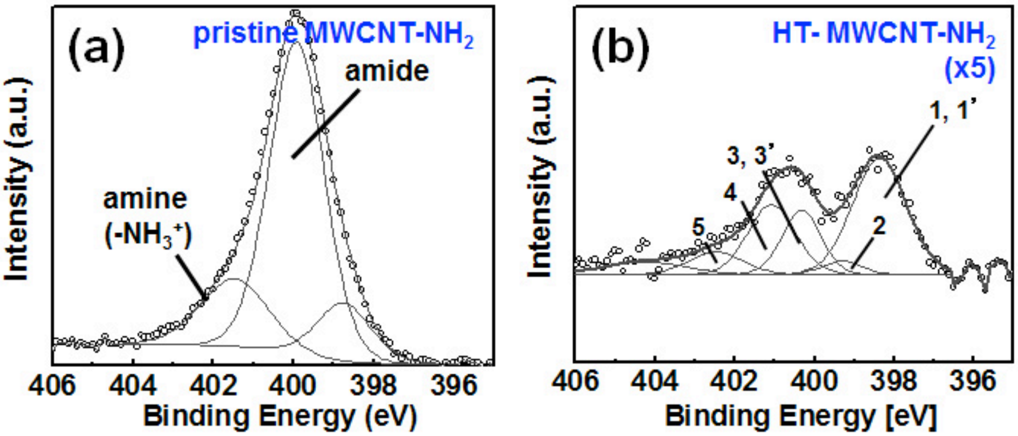

Fig. S9 Comparison of ORR mass activities of HT-MWCNT-NH_2 (pink), N-MWCNT (orange), 1-Fe-N-MWCNT (black), 2-Fe-N-MWCNT (green), and 3-Fe-N-MWCNT (blue) at 0.8 V vs. RHE as a function of (Fe+N)/C. The atomic ratio of Fe, N, and C were estimated from XPS (**Fig. 1** and **S6b**).

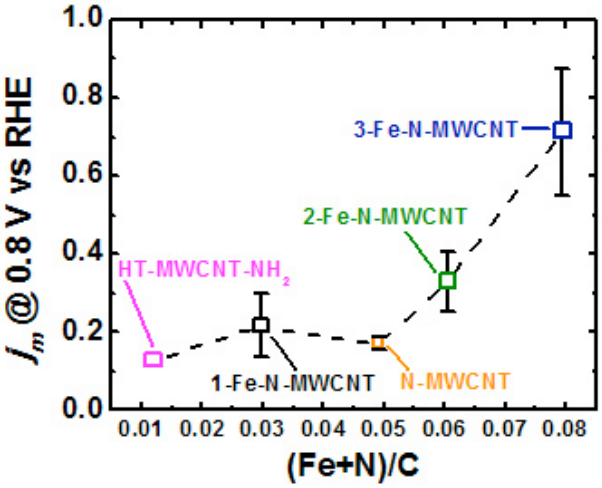

Fig. S10 The H_2O_2 amount (%H_2O_2) of N-MWCNT and 2-3 of Fe-N-MWCNTs with respect to the rotation rates and catalyst loadings in O_2-saturated 0.5 M H_2SO_4 at 10 mV s^{-1}. The rotation rates are 100 (green), 400 (red), 900 (black), 1600 (blue), and 2500 (pink) rpm. The maximum of %H_2O_2 values in Fe-N-MWCNTs are shown at 0.7 V vs. RHE, which is identical with reported Fe-N-C_{CB} catalysts[7]. The highest %H_2O_2 values in N-MWCNT are moved from 0.7 V (in 0.8 $mg_{N\text{-}MWCNT}$ $cm^{-2}{}_{geo}$) to 0.4 V vs. RHE (in 0.04 $mg_{N\text{-}MWCNT}$ $cm^{-2}{}_{geo}$). The %H_2O_2 values are generally independent on the rotation rates (100 - 2500 rpm) at high catalyst-loading (0.2 - 0.8 $mg_{catalyst}$ $cm^{-2}{}_{geo}$) while higher %H_2O_2 are obtained with decreasing rotation rate at low catalyst-loading (0.04 $mg_{catalyst}$ $cm^{-2}{}_{geo}$).

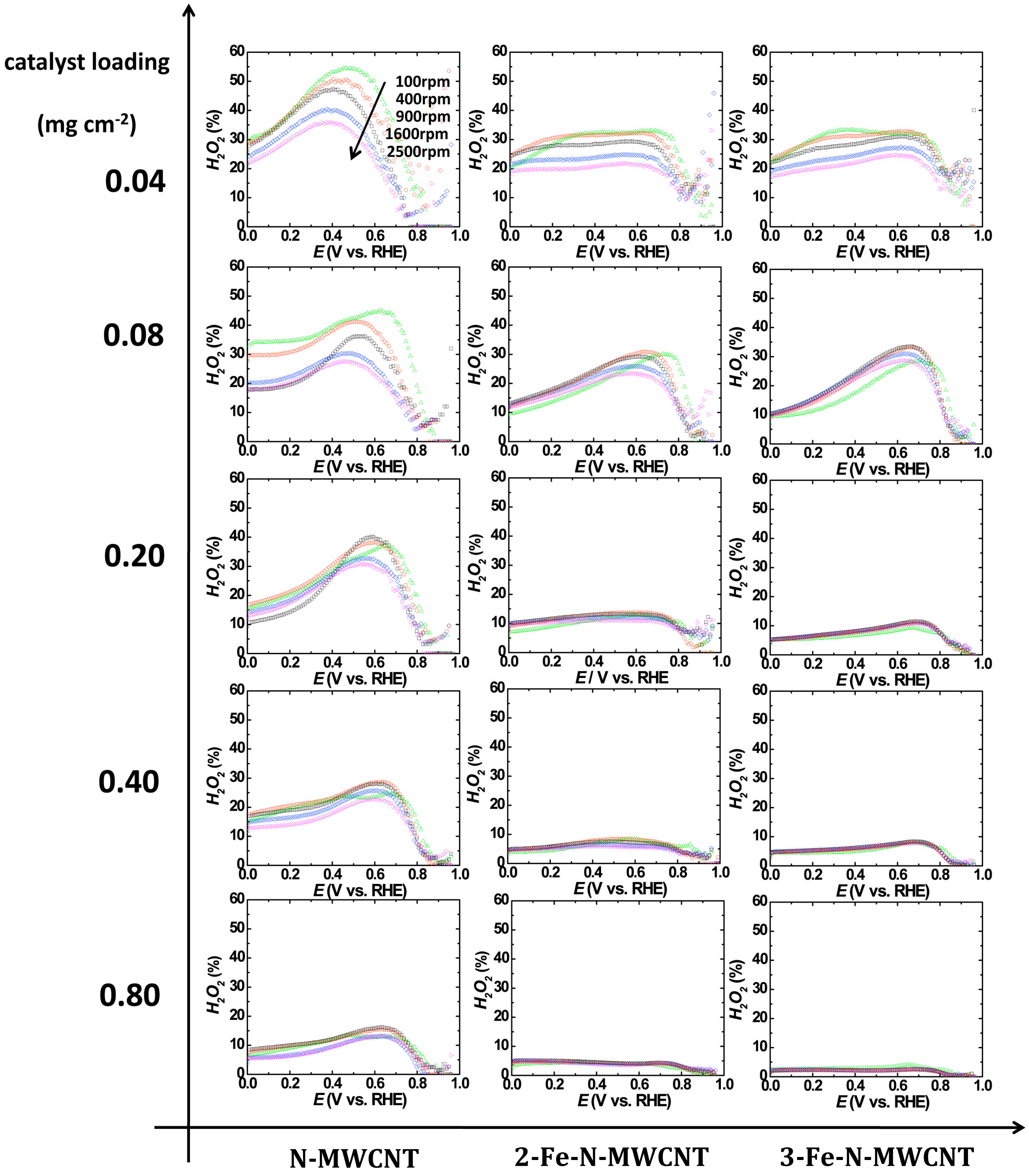

Fig. S11 %H_2O_2 of bare GC electrode, which has negligible %H_2O_2 at the potential range of 0.2 - 0.8 V vs. RHE, in O_2-saturated 0.5 M H_2SO_4 at 10 mV s^{-1}. The rotation rates are 100 (green), 400 (red), 900 (black), 1600 (blue), and 2500 (pink) rpm.

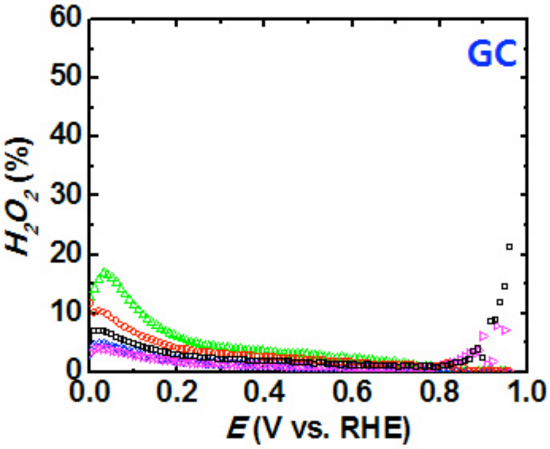

Fig. S12 ORR pathways in RRDE. (a) Diagrams of three oxygen reduction pathways. (**1**) is the direct 4-e transfer, and (**2**)-(**4**) are the indirect 4-e transfer where (**2**) is an initial 2-e transfer, (**3**) is the a peroxide electro-reduction, and (**4**) is a peroxide disproportionation. (b) %H_2O_2 and number of electron transferred as a function of catalyst loading in O_2-saturated 0.5 M H_2SO_4 at 10 mV s^{-1} and 900 rpm. Solid and dashed bars indicate 0.04 and 0.8 $mg_{catalyst}$ $cm^{-2}{}_{geo}$ of catalyst loadings, respectively. Fe-N-C_{CB} indicates %H_2O_2 values extracted from reference[7]. Error bars indicate a standard deviation from averaged %H_2O_2 of two samples.

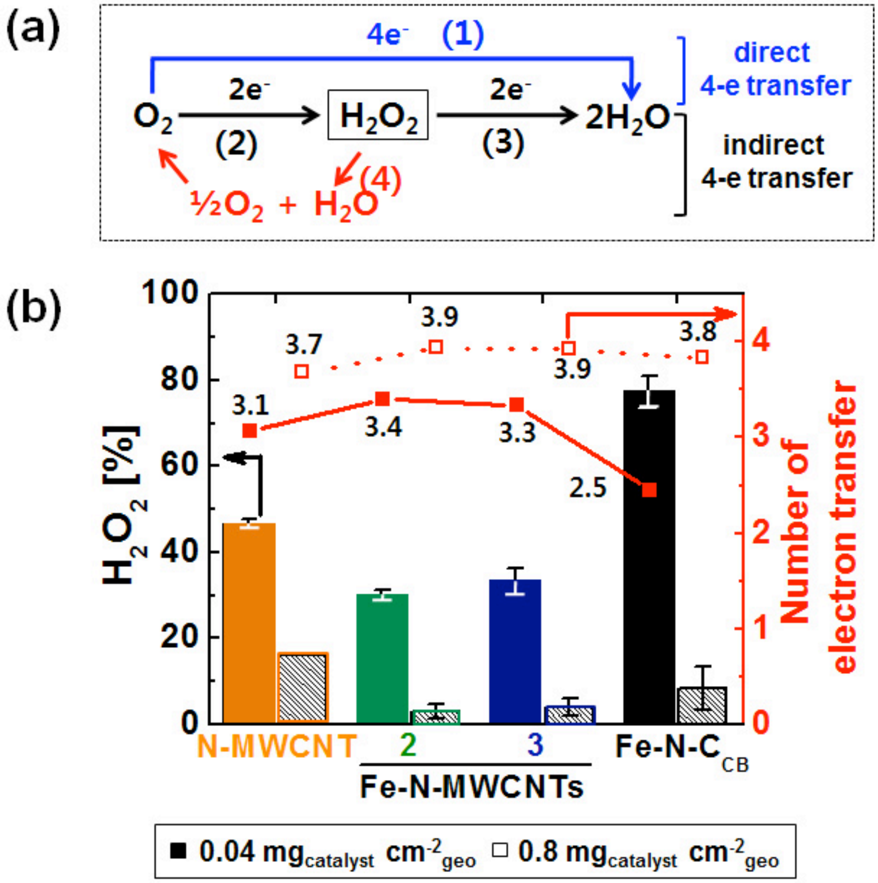

Fig. S13 The H_2O_2 oxidoreduction curves of (a) Pt-RDE, (b) N-MWCNT, (c) 2-Fe-N-MWCNT, and (d) 3-Fe-N-MWCNT in Ar-saturated 0.5 M H_2SO_4 with 1.3 mM of H_2O_2 (loading: 0.4 $mg_{catalyst}$ cm^{-2}_{geo}).[8] The potentials were swept from 1) the reduction scan (0.65 V to 0 V vs. RHE) to 2) the oxidation scan (0.65 V to 1 V vs. RHE) at 10 mV s^{-1}. The rotation rates of each sample are 100 (green), 400 (red), 900 (black), 1600 (blue), and 2500 (pink) rpm. The j_∞ values of Pt-RDE at 0.2 V vs. RHE are 0.71 - 2.82 $mA_{Pt\text{-}RDE}$ cm^{-2}_{geo} at 100 - 2500 rpm. The j_∞ values of samples at 0.5 V vs. RHE are ~0.08 $mA_{N\text{-}MWCNT}$ cm^{-2}_{geo} for the N-MWCNT, ~0.3 $mA_{2\text{-}Fe\text{-}N\text{-}MWCNT}$ cm^{-2}_{geo} for the 2-Fe-N-MWCNT, and ~0.3 $mA_{3\text{-}Fe\text{-}N\text{-}MWCNT}$ cm^{-2}_{geo} for the 3-Fe-N-MWCNT at 400 - 2500 rpm.

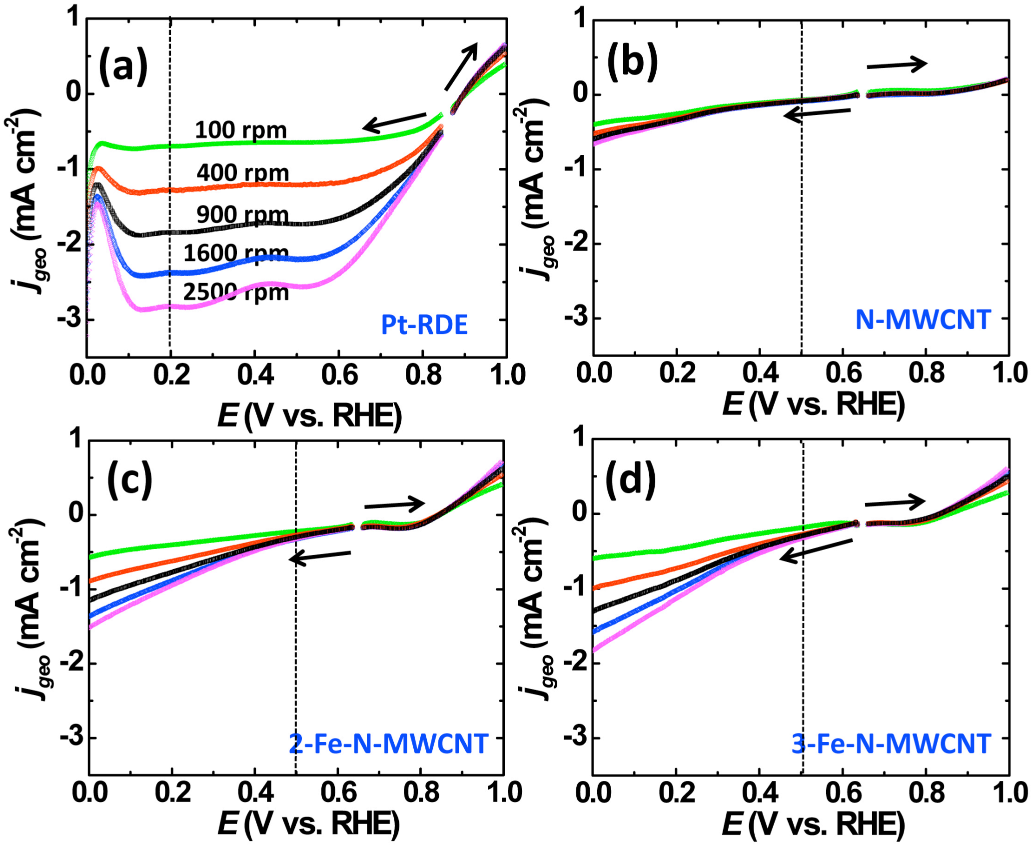

References

1. K. Jurewicz, K. Babeł, A. Źiółkowski and H. Wachowska, *Electrochim. Acta*, 2003, **48**, 1491-1498.
2. F. Jaouen, J. Herranz, M. Lefevre, J. P. Dodelet, U. I. Kramm, I. Herrmann, P. Bogdanoff, J. Maruyama, T. Nagaoka, A. Garsuch, J. R. Dahn, T. Olson, S. Pylypenko, P. Atanassov and E. A. Ustinov, *ACS Appl. Mater. Interfaces*, 2009, **1**, 1623-1639.
3. J. Machnikowski, B. Grzyb, J. V. Weber, E. Frackowiak, J. N. Rouzaud and F. Béguin, *Electrochim. Acta*, 2004, **49**, 423-432.
4. T. Ramanathan, F. T. Fisher, R. S. Ruoff and L. C. Brinson, *Chem. Mater.*, 2005, **17**, 1290-1295.
5. S. W. Lee, B. S. Kim, S. Chen, Y. Shao-Horn and P. T. Hammond, *J. Am. Chem. Soc.*, 2009, **131**, 671-679.
6. F. Charreteur, F. Jaouen and J. P. Dodelet, *Electrochim. Acta*, 2009, **54**, 6622-6630.
7. A. Bonakdarpour, M. Lefevre, R. Z. Yang, F. Jaouen, T. Dahn, J. P. Dodelet and J. R. Dahn, *Electrochem. Solid State Lett.*, 2008, **11**, B105-B108.
8. F. Jaouen and J. P. Dodelet, *J. Phys. Chem. C*, 2009, **113**, 15422-15432.